Electronic Supplementary Information

Cascade targeting tumor mitochondria with CuS nanoparticles for enhanced photothermal therapy in the second near-infrared window

Haiyan Wu,†[a,b] *Pengpeng Jia,*†[a,c] *Yu Zou,*[a,c] *and Jiang Jiang*[*a,c]

[a] *i-Lab and Division of Nanobiomedicine, CAS Key Laboratory of Nano-Bio Interface, CAS Center for Excellence in Nanoscience, Suzhou Institute of Nano-Tech and Nano-Bionics, Chinese Academy of Sciences, Suzhou 215123, China.*

[b] *Nano Science and Technology Institute, University of Science and Technology of China, Suzhou 215123, China*

[c] *School of Nano-Tech and Nano-Bionics, University of Science and Technology of China, Hefei 230026, China*

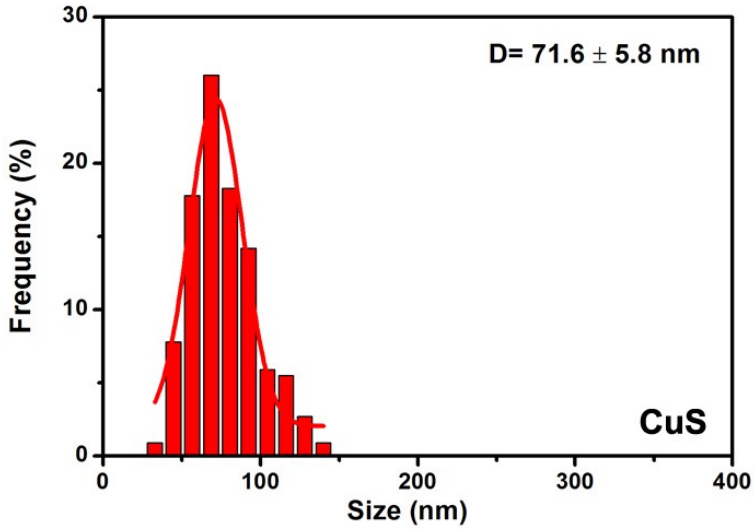

Fig. S1 Size distribution histogram of CuS NPs determined by TEM images.

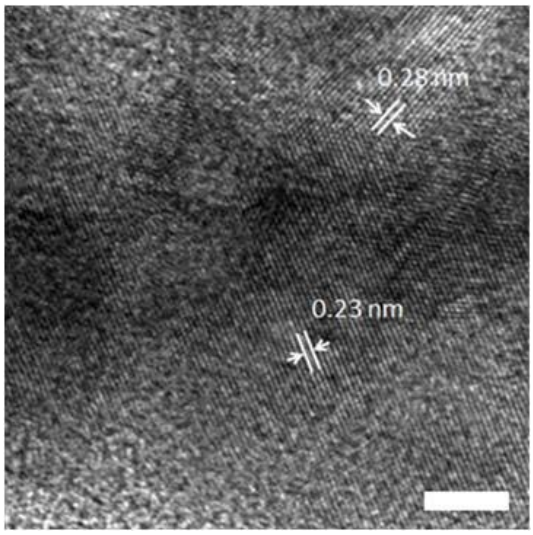

Fig. S2 HRTEM image of CuS NPs showing characteristic lattice spacings, scale bar: 5 nm.

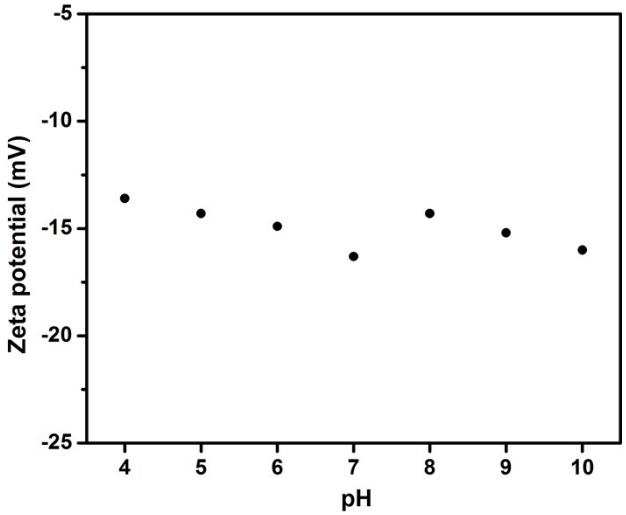

Fig. S3 Zeta potential of CuS-TPP-HA NPs solution between pH 4 and 10.

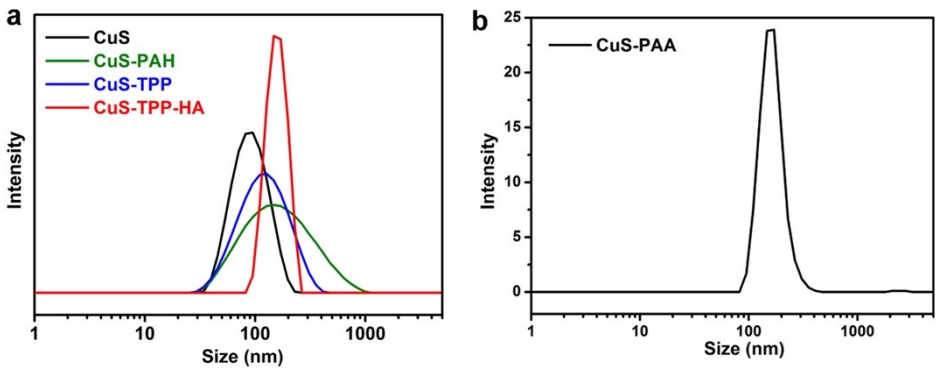

Fig. S4 Dynamic light scattering (DLS) characterizations of (a) CuS NPs with different surface functioning molecules and (b) reference CuS-PAA NPs.

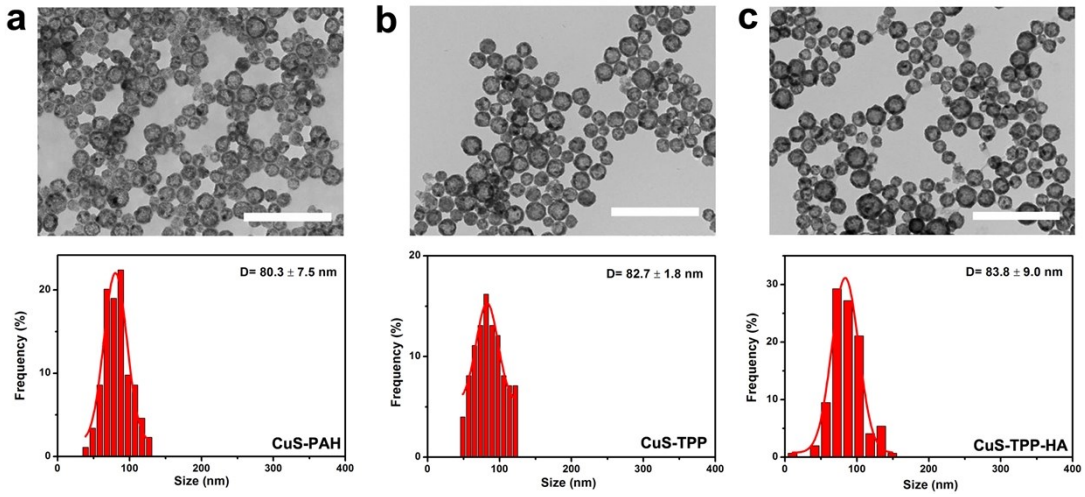

Fig. S5 TEM images and size distribution histograms of (a) CuS-PAH, (b) CuS-TPP, and (c) CuS-TPP-HA NPs. Scale bars: 500 nm.

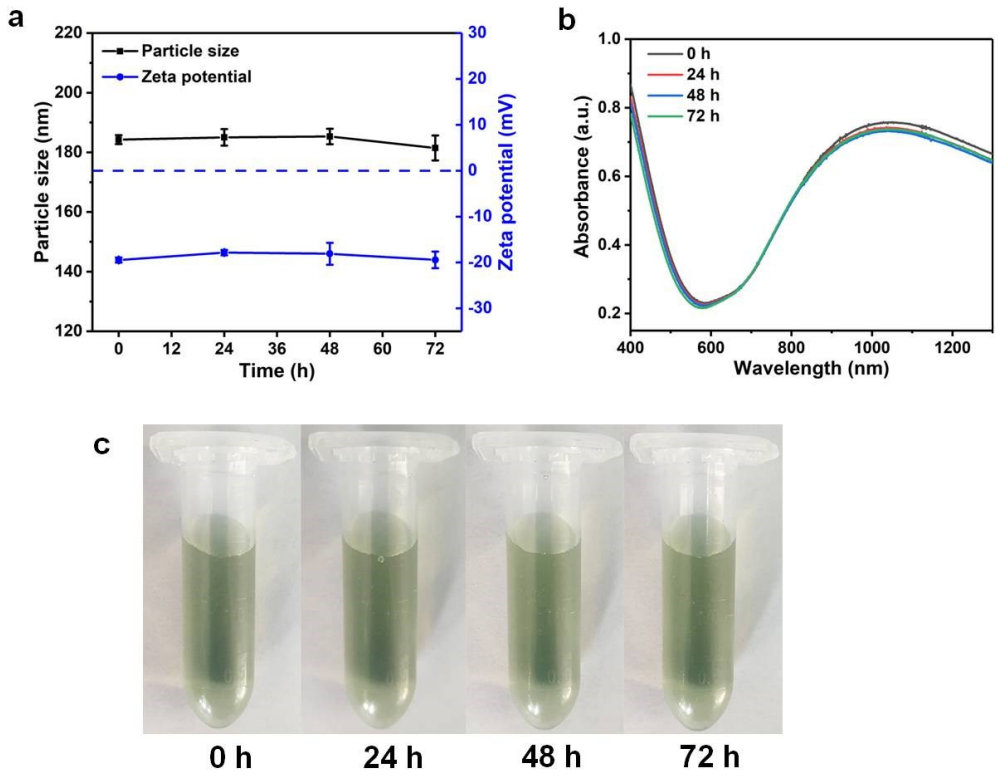

Fig. S6 (a) Hydrodynamic size and zeta potential, (b) UV-vis-NIR absorption, and (c) visual inspection of CuS-TPP-HA NPs solution over the course of 3 days.

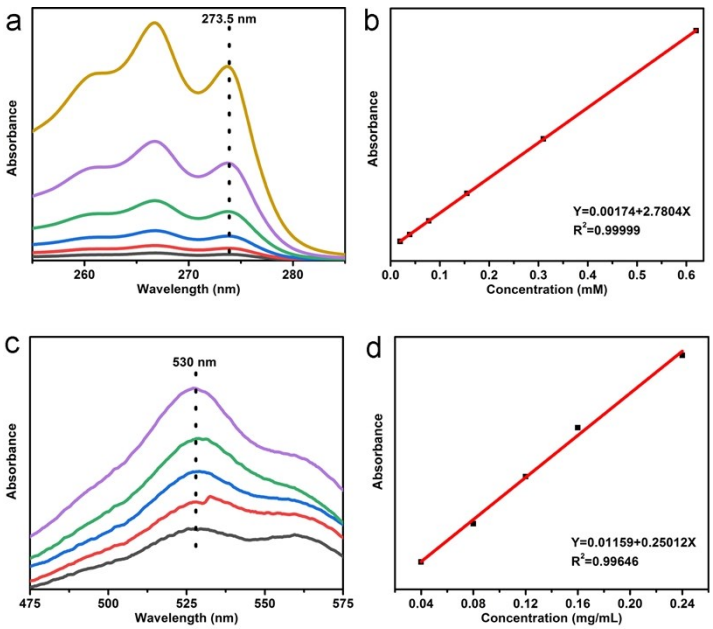

Fig. S7 (a) Absorption spectra of different concentration TPP solution, and (b) the linear fit of absorbance at 273.5 nm as a function of TPP concentrations. (c) The absorption spectra and (d) calibration curve of HA solution based on the Elson-Morgan method.

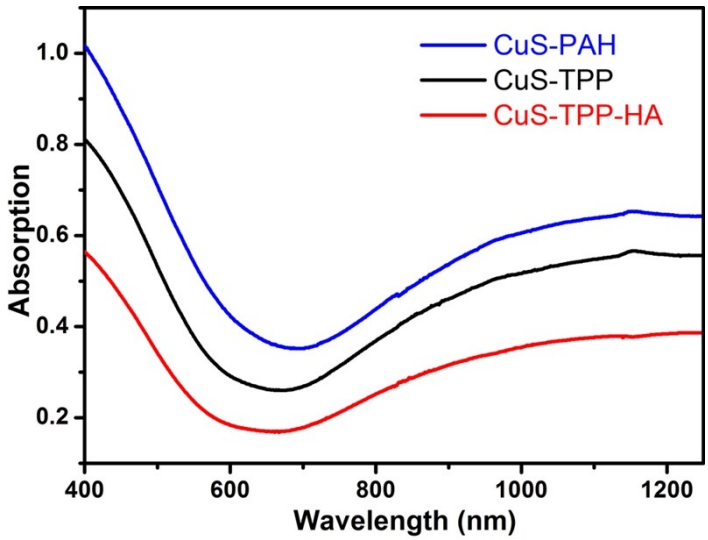

Fig. S8 UV-vis-NIR absorption spectra of CuS NPs with different surface functional layers. The curves have been shifted arbitrarily in the vertical axis for better viewing purpose.

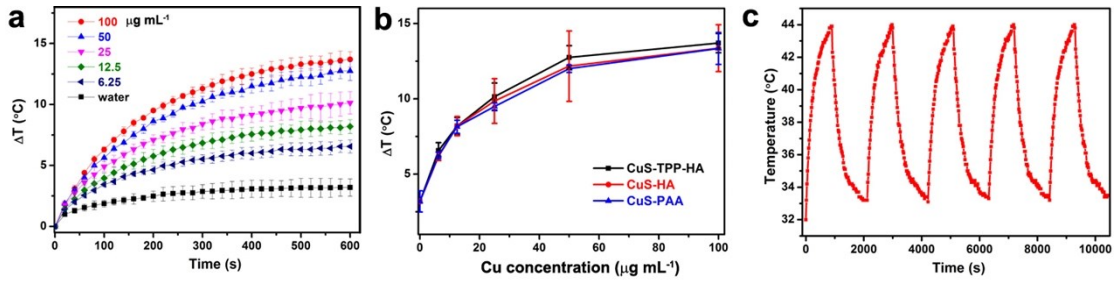

Fig. S9 (a) Photothermal heating curves of CuS-TPP-HA NPs solution at various concentrations when being exposure to light irradiation (1064 nm, 0.75 W cm^{-2}, 10 min). (b) Final solution temperature elevation at the end of 10 min laser exposure as a function of Cu concentrations for different surface protected CuS NPs. (c) Temperature variations of five heating/cooling photothermal cycles of CuS-TPP-HA NPs solution.

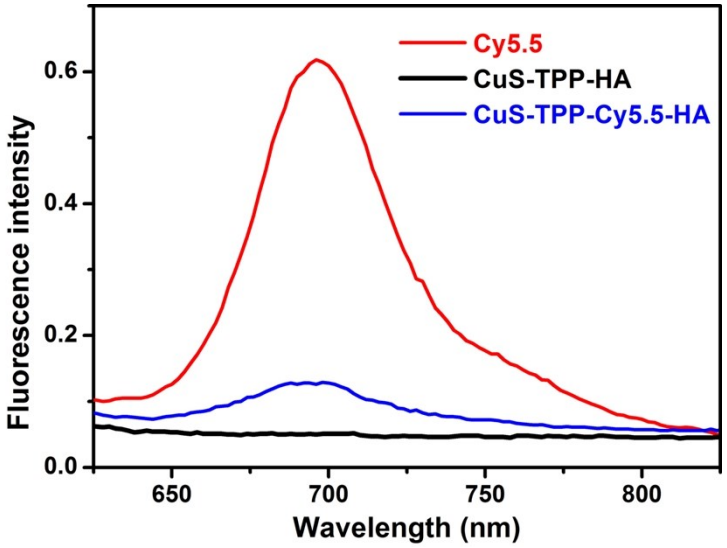

Fig. S10 Fluorescence spectra of Cy5.5, CuS-TPP-HA NPs, and Cy5.5 labeled CuS-TPP-HA NPs solutions.

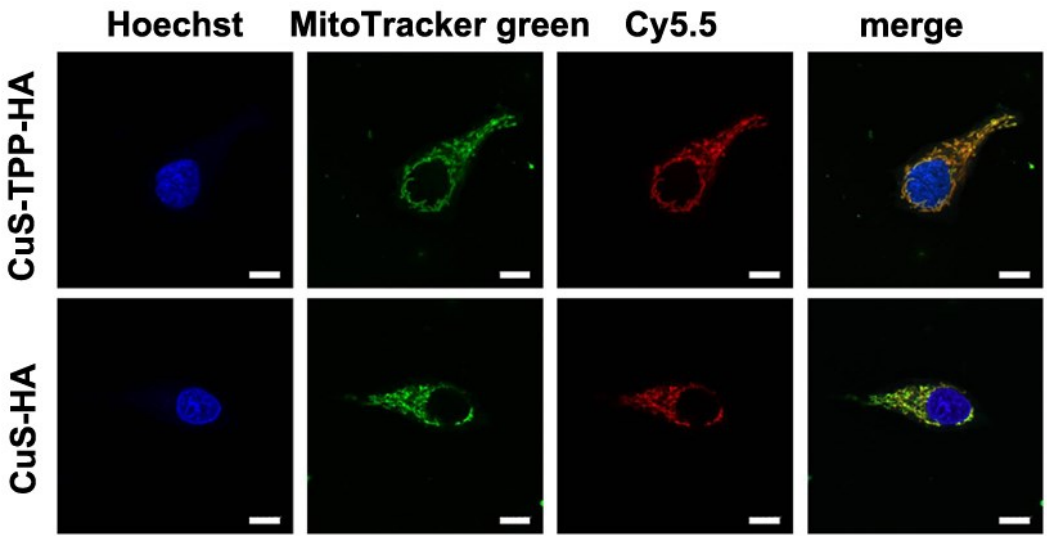

Fig. S11 Confocal fluorescence images of MCF-7 cells incubated with CuS-Cy5.5-HA and CuS-TPP-Cy5.5-HA NPs for 4 h, with Hoechst and MitoTracker Green co-labeling nuclei and mitochondria, scale bars: 10 μm.

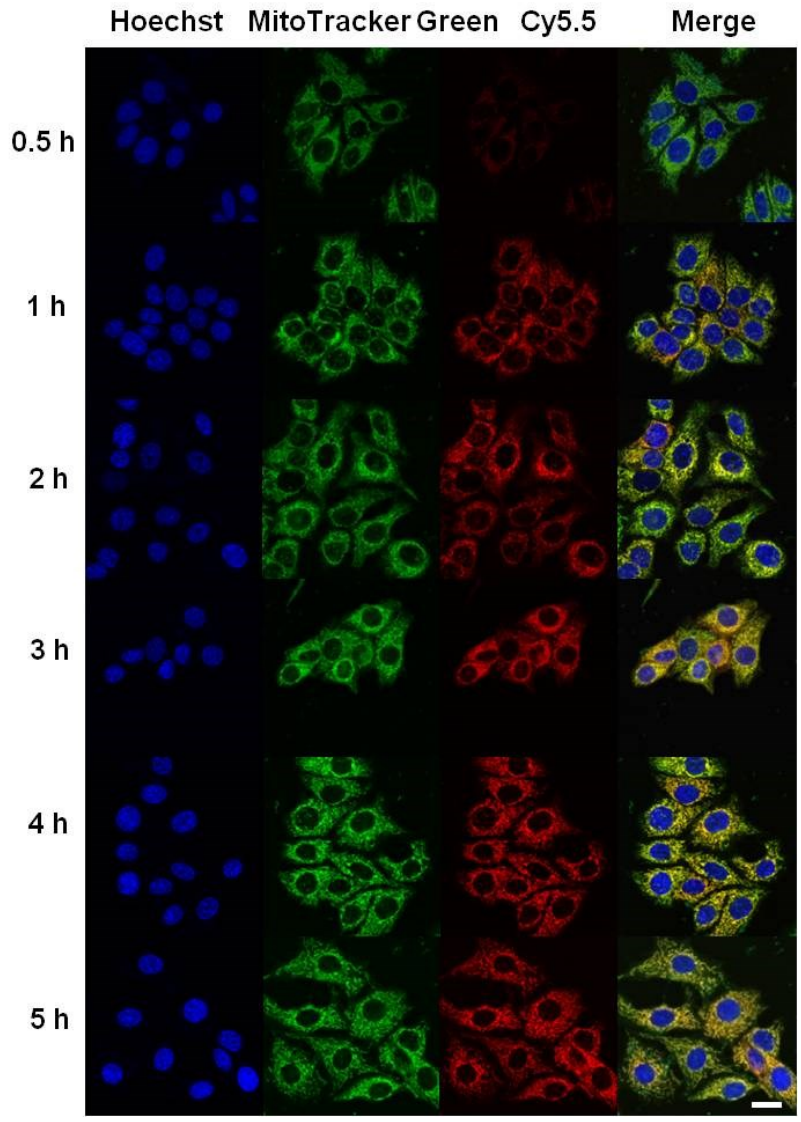

Fig. S12 Confocal fluorescence images of MCF-7 cells incubated with CuS-TPP-Cy5.5-HA NPs for different durations, while nuclei and mitochondria were co-stained using Hoechst and MitoTracker Green, scale bar represents 20 μm.

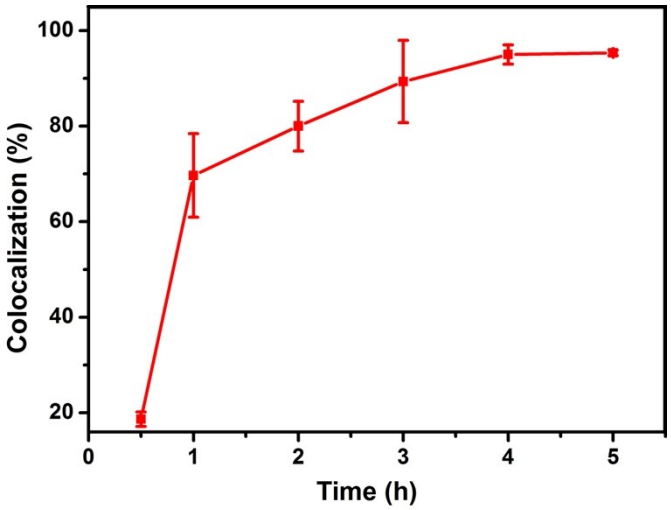

Fig. S13 Calculated co-localization coefficient of green (MitoTracker Green) and red (Cy5.5) fluorescence shown in Fig. S12 as a function of time.

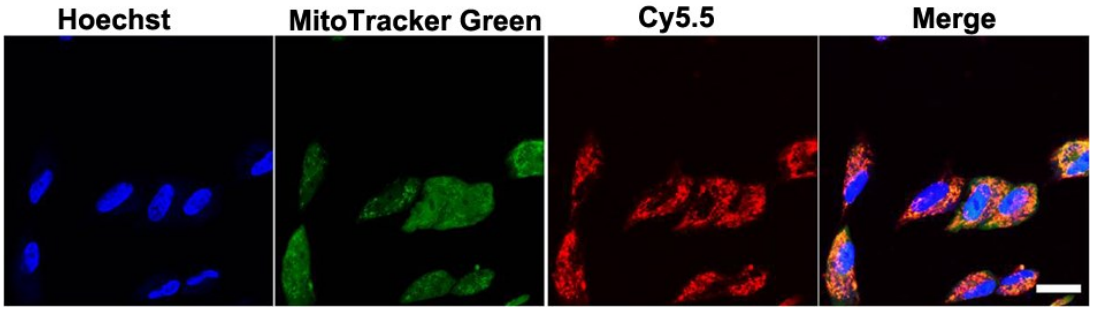

Fig. S14 Confocal fluorescence images of HFF cells incubated with CuS-TPP-Cy5.5-HA NPs for 4 h, while nuclei and mitochondria were co-stained using Hoechst and MitoTracker Green. The calculated co-localization coefficient is 49%. Scale bar: 20 μm.

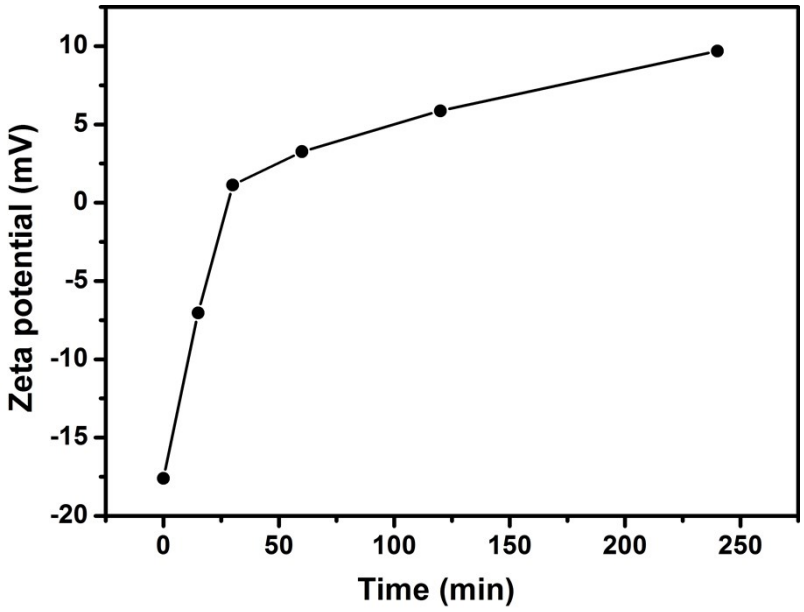

Fig. S15 Temporal evolution of the zeta potentials of CuS-TPP-HA NPs co-incubated with HAase (at time 0).

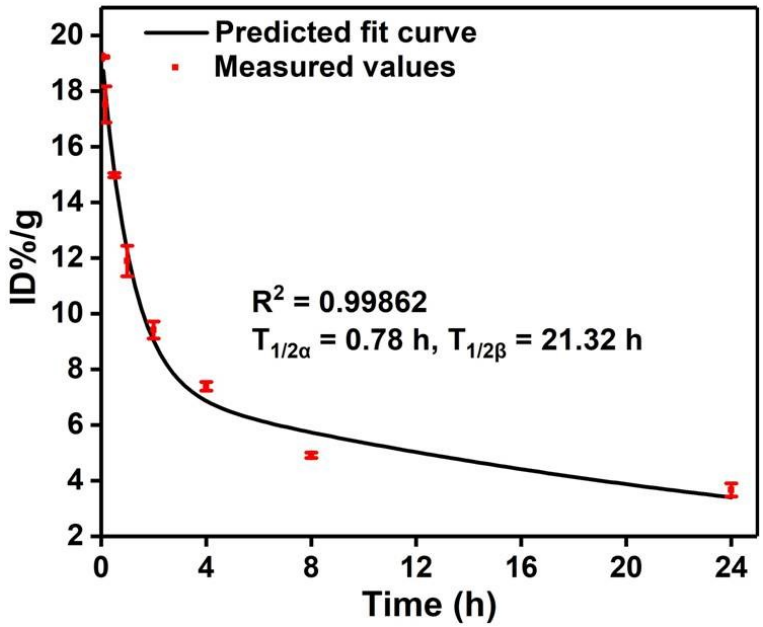

Fig. S16 Blood circulation profile of CuS-TPP-HA NPs as determined by ICP quantifications, the fitting is based on a two-compartment model.

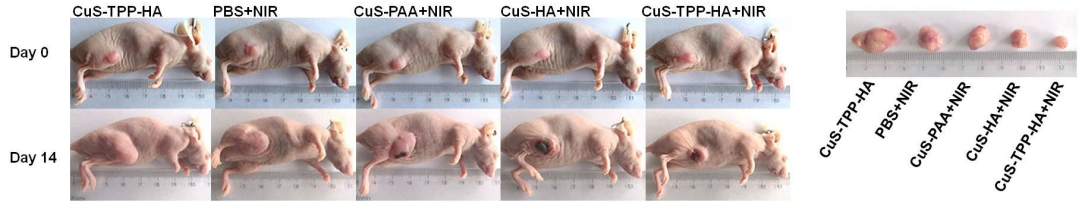

Fig. S17 Photographs of the xenograft tumors at day 0 and day 14 after various treatments, and the dissected tumors after sacrificing mice 14 days post photothermal therapy.